1 OF 1

AD
A064857

END
DATE
FILMED
4-79
DDC

LEVEL # 0

ADA064857

6 CLOUD CHAMBER INFRARED MEASUREMENTS

9 Final Report
Contract No. DAAK70-76-C-0246
15

11 January, 1978

by

10 Daniel R. White

12 43p.

prepared for

Department of the Army
U.S. Army Mobility Equipment Research and Development Command
Night Vision Laboratory
Ft. Belvoir, Virgina 22060

D D C

JAN 25 1979

A

400 144

79 01 23 492

ABSTRACT

During the ~~period, of this contract~~ report period, the design of the simulation chamber ~~has been~~ was established, initial thermal tests ~~have been~~ were conducted, and a study of the procedure for making the desired IR attenuation and scattering measurements ~~has been~~ was made. Limitations of both time and funds have not permitted the project to be carried through to the point of making actual IR measurements.

The project is being continued subject to available funding from a variety of sources.

page - i -

79 01 23 492

R78-0395

I. Introduction

The overall program of work planned for this project
includes:

1) Design of a full size cloud simulation chamber,
2) Construction and performance testing of a single section
   of the chamber, and
3) Attempt to make scattering and attenuation measurements
   of infrared radiation in clouds and fogs.

Success has varied widely between the three items. Item
1 has been the most successful with completion of the design
of the major chamber parts; however, numerous details associated
with support hardware are yet to be decided. Item 2 has been
limited to work with a small test section representing one-
twenty fourth of a chamber side wall section. Work on Item
3 has consisted of some feasibility studies and planning for
procedures required.

II. Description of work

A. Design of full size cloud simulation chamber

The current design of the full size cloud simulation
chamber is given in the accompanying set of machine shop
drawings. The basic approach has been changed from a two
phase refrigeration cooling system for temperature control
of the interior wall surface to a thermoelectric cooled
inner wall. The thermoelectric design has always been
the preferred technique based on versatility, compute com-
patibility, speed of response, quality and ease of control.
However, at the time the proposal was submitted, calcula-
tions of interior surface temperature uniformity as a
function of inner wall thickness predicted the need for
a 2.54 cm. thick inner wall to meet required uniformity
tolerances, this resulted in an effective heat capacity
per thermoelectric module which made it impossible to meet
the required maximum cooling rate of 15°c/min. We have
since circumvented the problem by using a laminated alum-
inum inner wall having an anisotropic thermal conductivity.

This combines the smoothing properties of the thick plate with the smaller heat capacity of a thin plate.

The initial design was then developed based on previous computer heat transfer studies, experience gained from work with the present prototype chamber, and mechanical and fabrication restrictions. A pictorial drawing of the complete chamber is shown in Fig. 1. The chamber consists of flat top and bottom plate assemblies and seven cylindrical side wall assemblies which can be stacked in any sequence. This permits modifications made to one section to be used at any level of the chamber.

Fig. 2 shows a cross section of a side wall. The inner wall plate is formed by bonding a 6.35mm aluminum plate and a 3.17mm aluminum plate together with "Melt Bond 1133" (Narmco Materials, Inc., Costa Mesa, CA). The outer 5.72cm aluminum wall serves as a heat sink for the thermoelectric modules, therefore heat transfer from the heat sink to the inner wall past the thermoelectrics must be minimized. The studs extending from the inner wall plate out through the heat sink provide the compression necessary for proper heat transfer to and from the thermoelectric modules. The O-ring seal around the perimeter of the inner wall plate together with those around the expansion parts form part of the primary chamber sensitive volume seal. The seals around the studs and inner wall thermometer serve as a secondary seal to permit maintainence of a vacuum around the thermoelectric modules. This reduces the reverse heat flow from the heat sink to the inner wall.

The temperature of the heat sink is maintained by a flow of thermally regulated liquid through passages located near the outer surface. The passages are interconnected in pairs so that liquid which flows down one passage returns through the adjacent passage, both passages are behind a single row of thermoelectric modules. The double-back flow pattern compensates for the increase in liquid temperature as it passes through the heat sink. The resulting

heat sink temperature as seen by the thermoelectric modules
is the average of the inlet and outlet temperatures. Flow
paths are verticle in the side walls and parallel to the
long dimension of the inner wall plates on the top and bottom.
The external manifolding, only a portion of which is shown
in Fig. 1, is designed so that a given volume of liquid
makes only a single pass through the heat sink before being
returned to the main reservoir. Each of the nine major
chamber assemblies forms an independent flow path between
the main inlet and return lines, this insures adequate flow
in all units regardless of the number in use. It is es-
timated that a flow of 1.4 l/sec per section will be required
at maximum cooling.

The expansion of the sensitive volume is accomplished
by drawing air out through numerous small ports evenly
distributed over the chamber side walls. Each interior
side wall plate contains thirty-six parts. The external
manifolding has been designed to produce equal air flow
through all ports. This results in an expansion of the
sensitive volume in which air motion is confined to the
horizontal plane with radial symmetry about the central
axis of the chamber. Any vertical air motion caused by
the discrete nature of the ports is localized in the vicinity
of the walls with an average of zero. The flow calcula-
tions used to determine passage sizes in the external mani-
folds are given in Appendix A.

The expansion manifold will also be used for sample
introduction. All the individual manifold layers, only
a portion of which are shown in Fig. 1, are connected by
four vertical mains spaced at 90° intervals around the
chamber. If these mains are clocked just above the bottom
side wall assembly and just below the top side wall assembly
any air flow entering the system at the bottom and being
exhausted at the top will have to pass through the sensi-
tive volume. This technique eliminates the mechanical
complexity and thermal anomally of separate sample inlet

and outlet ports. Theoretical calculations of the effects
on aerosol size distribution caused by passage through the
inlet maniforld are given in Appendix B.

B. Construction and Thermal Tests

Once the basic design of the heat sink and inner wall
was decided, a small test section was constructed. This
unit represents half of one of the twelve faces of a side
wall assemb16. This also represents the interior surfaces
which are cooled by a single controller-power supply unit.
The test section has twenty thermoelectric modules (Barg
Warner Thermoelectric - Model 940-31) mounted in a 4 by 5
rectangular array. In the full size chamber, each of the
twelve faces of a side wall assembly will have fourty
thermoelectric modules in a 4 x 10 array with each of the
two 4 x 5 halves having its own controller-power supply.

The controller-power supplies developed for the current
prototype chamber do not have either the voltage or current
capability to provide full power to twenty thermoelectric
modules (14 amps @ 70 VDC). This forced us to use manual
control for all tests with the power supply in either the
constant current or constant voltage mode.

The first test was a measure of the maximum cooling
rate to insure that the required 15°c/min could be achieved.
The results showed that for as much as 10°c below the heat
sink temperature, the inner wall could be cooled at rates
in excess of 15°c/min. Rates as high as 25°c/min were
measured for wall temperatures very near the heat sink
temperature. These results should be taken as a minimum
performance test since they were conducted without a
vacuum between the inner wall and heat sink, and we were
still searching for the optimum thermal contact between
the thermoelectrics and adjacent surfaces. The measurements
were made using one of the transistor thermometers developed
in this laboratory (See Appendix C) mounted in a smooth
hole boxed in the inner wall plate. The sensor response
time may have lowered the maximum measured cooling rate.

5

The sensor mount has since been redesigned and the response time reduced from approximately 7 seconds to approximately 4 seconds.

The next tests were to measure the uniformity of surface temperature of the inner wall plate as a function of thermoelectric current. Plans to photograph the location of hot or cold spots depicted by a sheet of liquid crystal paper attached to the front of the inner plate failed due to difficulty in achieving a uniform contact between paper and plate and effects of the ambient temperature on the uninsulated surface. Thin film thermocouples were attached to the surface of the inner wall plate representing the interior chamber wall in the configuration shown in Fig. 3. The dotted squares show the location of the thermoelectric modules, the x's are the thermocouple locations and the circle is the transistor thermometer. The test section was insulated with three layers of polyethylene foam 1.27 cm thick laminated with two layers of aluminum foil. The foam has a thermal conductivity of 0.036 W/MK. The heat sink coolant was water circulated through a closed loop system containing a refrigerated heat exchanger for removal of the excess heat. The test section was supported in an upright position to duplicate the orientation in the final assembly and to insure that the coolant passages remained filled with water.

During the tests, the power supply for the thermoelectrics was adjusted to provide the desired current, then the system was allowed to cone to a steady state condition. At this point the temperature difference between the two surface points being tested was recorded. The results for the three measured differences are shown in Fig. 4 for currents up to 7 amps. The difference ΔT_{23} is in the expected direction and while slightly larger than desired, is small enough to work with since it represents a short range ripple which will be smoothed out only a short distance from the wall.

While not tested at this time, it is felt that the major contribution to the differences ΔT_{21} and ΔT_{24} was caused by the need to parallel the wiring of horizontal rows of thermoelectric modules. This was due to voltage limits of the power supplies available. Our previous experience with parallel wiring has shown that this can happen due to slight differences in the electrical resistance of different modules. It should be noted that the difference $\Delta T_{14} = \Delta T_{24} - \Delta T_{21}$ remains small. Other possible sources requiring further investigation are variations in heat sink temperature, convection of the air surrounding the thermoelectric modules, and variations in thermoelectric compression force. Further tests at higher currents and with all units in series are also required.

C. Infrared Scattering and Attenuation

The transparency of the atmosphere which makes infrared radiation so useful for detection, surveillance, electrooptical control and guidance applications is the same feature which makes laboratory measurements of attenuation so difficult. Typical attenuation measurements are made using optical paths of kilometer length to provide sufficient attenuation to achieve an adequate signal to noise ratio. However, this makes it impossible to measure the atmospheric parameters along the entire path with the desired accuracy if a straight line path is used. The cloud simulation chamber being designed can provide the required knowledge of the atmospheric parameters but puts severe restrictions on the physical size of the system.

By utilizing windows located in the top and bottom of the chamber, a physical path length of 2.85m can be obtained. The proposed window design (see machine drawings) is compatible with use in both the top and bottom plates as well as the side walls. The design also permits the addition of extra windows with relatively simple modifications.

Some preliminary tests using a low power CW laser

operating in the visible red have led to the conclusion
that it is feasible to utilize a white cell to obtain
a large number of reflections of the beam between two
spherical mirrors. This would permit the optical path
length to be increased to the required lengths while re-
maining within the physical constrains of the chamber.
The tests also indicated that the system should be rela-
tively easy to align. Small change in alignment occuring
during uses should not greatly effect operation.

In the case of scattering, measurements will be made
using a horizontal beam through the chamber. The initial
side wall design places windows at relative angles of 0°,
30°, 90°, 180°, 210°, and 270° around the chamber; however,
if necessary additional windows at any multiple of 30°
can be added with relative ease. It is not expected that
the scattering measurements will require a multipass op-
tical path but this would not cause any major problem if
necessary.

An examination of the present technology of IR sources
and detectors appears to indicate the use of one of two
basic choices. In one case, the source would consist of
a standard and relatively inexpensive black body or globar
which are physically large and produce a low intensity.
These sources would require at least a liquid nitrogen
cooled detector (mercury cadmium telluride) resulting
in an expensive sophisticated system requiring constant
maintainance. The other case would use a relatively in-
expensive pyroelectric detector (lithuim tantalate or
polyvinylidene fluoride) but would need one of the high
intensity laser diodes or IR tunable lasers, both of which
are still relatively new and expensive. The present lasers
also require constant attention from a highly qualified
research staff member.

While the statements above seem to give little help
in choosing between the two systems, we are currently
planning on using the pyroelectric detector and either

laser or laser diode source for two reasons. First, as the development of both the IR tunable laser and laser diodes progresses, they will undoubtedly become more reliable, easier to maintain, and less expensive. There appears to be little reason to expect any significant changes in their areas with the liquid nitrogen cooled detectors. Second, by using an existing CO_2 laser at 10 microns, the system can be designed, tested, and initial data at 10 microns collected prior to the expendure of funds for the most expensive part of the system.

The use of the existing CO_2 laser would also permit the development of the optics to be pushed ahead separate from the chamber construction thereby permitting early solution to such problems as aerosol collection on mirrors and windows. The completed system would then be transferred to the chamber when required.

III. Summary and Future Work

During the period covered by this contract, we have completed the design of the major chamber components, performed the initial thermal tests of the design, made a comparative survey to determine the best choice of optical system, and made preliminary tests to further verify the feasibility of making IR attenuation measurements in the chamber. Limitations of both time and funds have prevented us from progressing beyond these early stages to the point of making actual measurements of either IR scattering or attenuation at this time. Based on the work completed to date, we are confident that the cloud simulation chamber being developed here can provide the type and quality of atmospheric radiation measurements required to support the work of the Night Vision Laboratory.

It is our current plan to continue with the development and construction of the chamber described in this report. Due to the versatility of the chamber, funds are being sought from a number of federal agencies and several private corpora-

tions which have interests in areas of atmospheric research which could benefit from work with this chamber. We also feel that the size of the total project which has a current estimated budget of $1.25 million dollars over a four year period would be beyond the resources of any one agency interested in this area of research. In developing the present budget and schedule estimates we have tried to be as realistic and complete as possible at this time.

At the present time pending additional funding, we are continuing the project using whatever funds and manpower can be spared from our other projects.

1
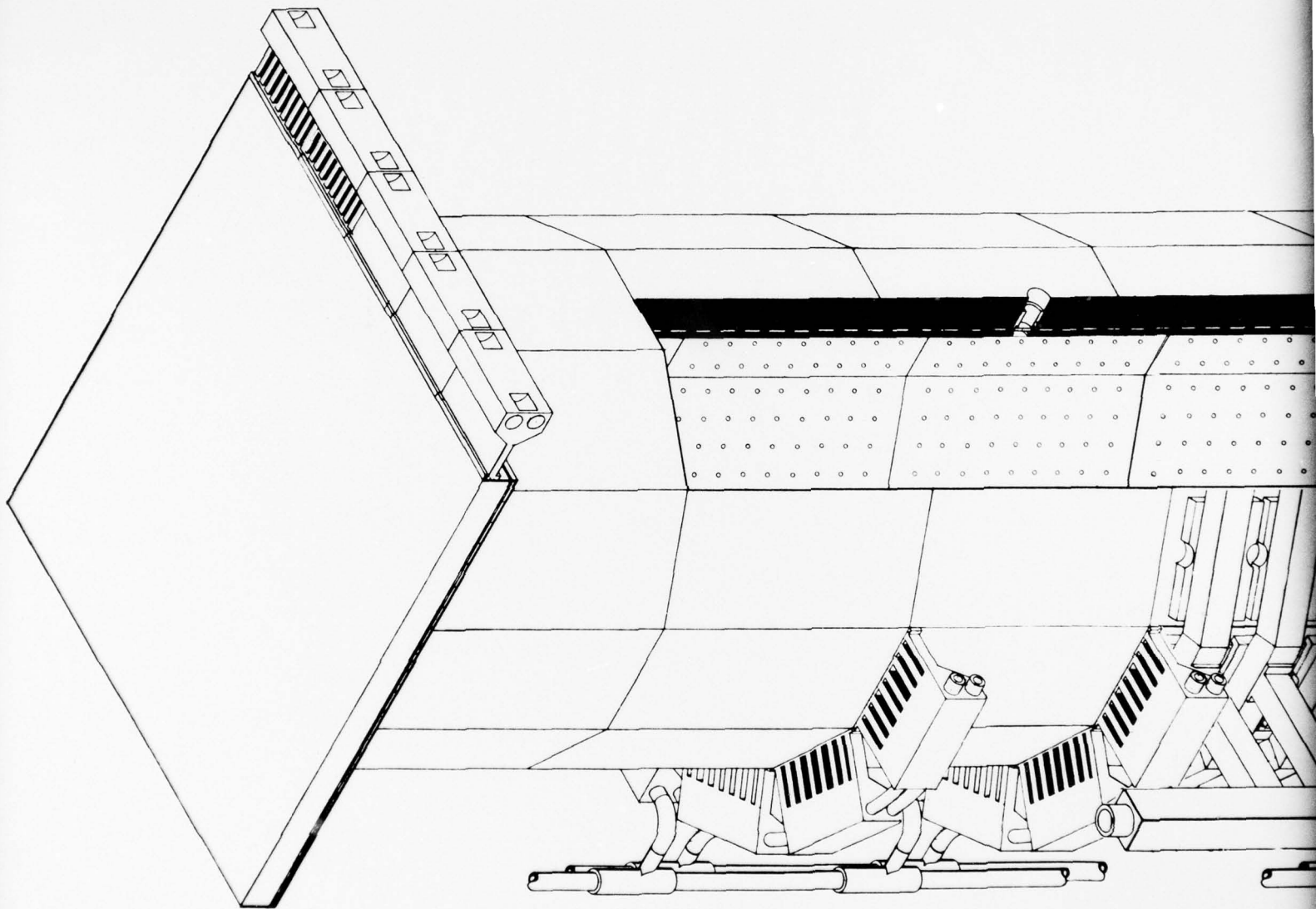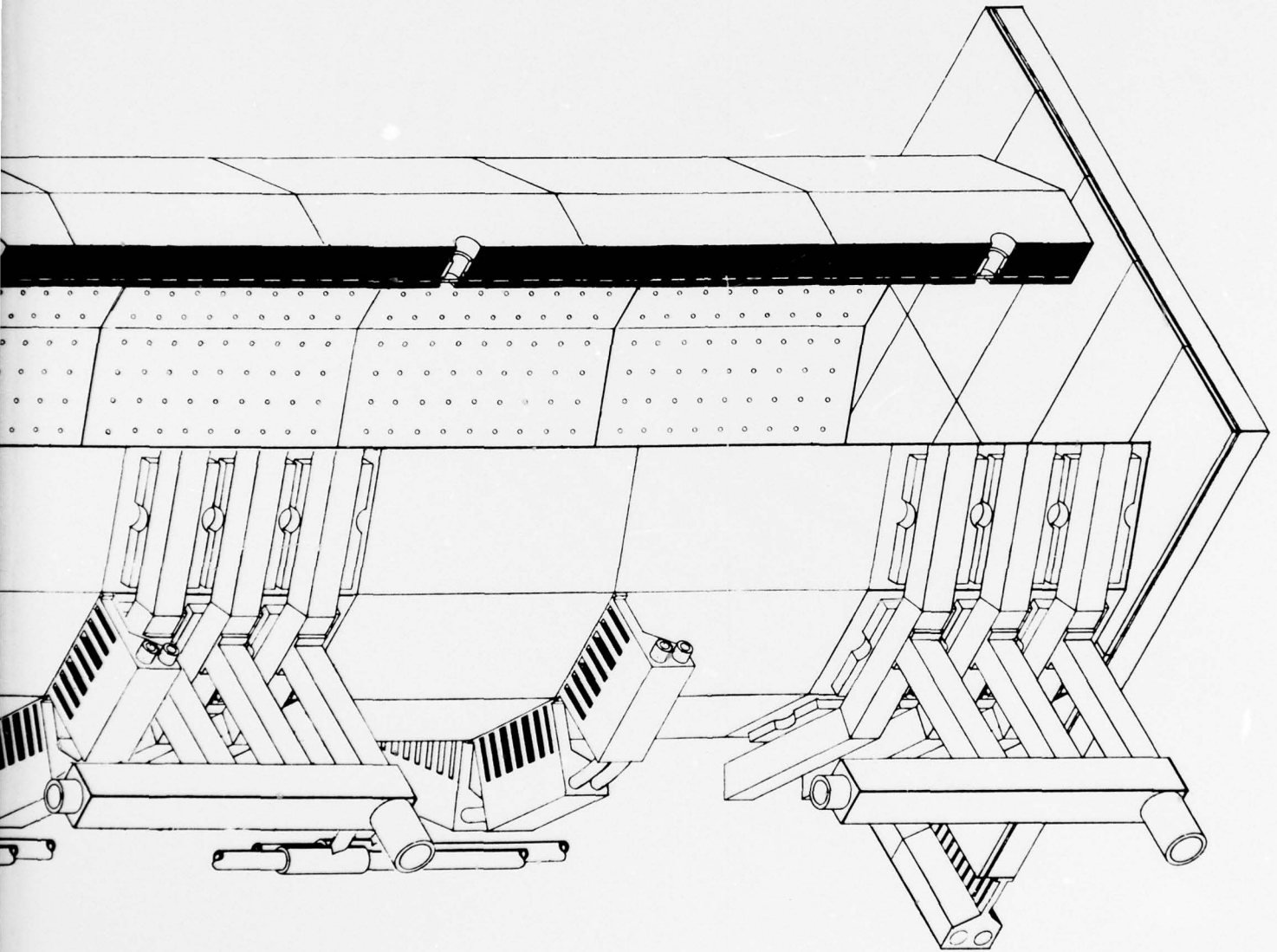
Fig. 1 Cloud Simulation Chamber

2

11
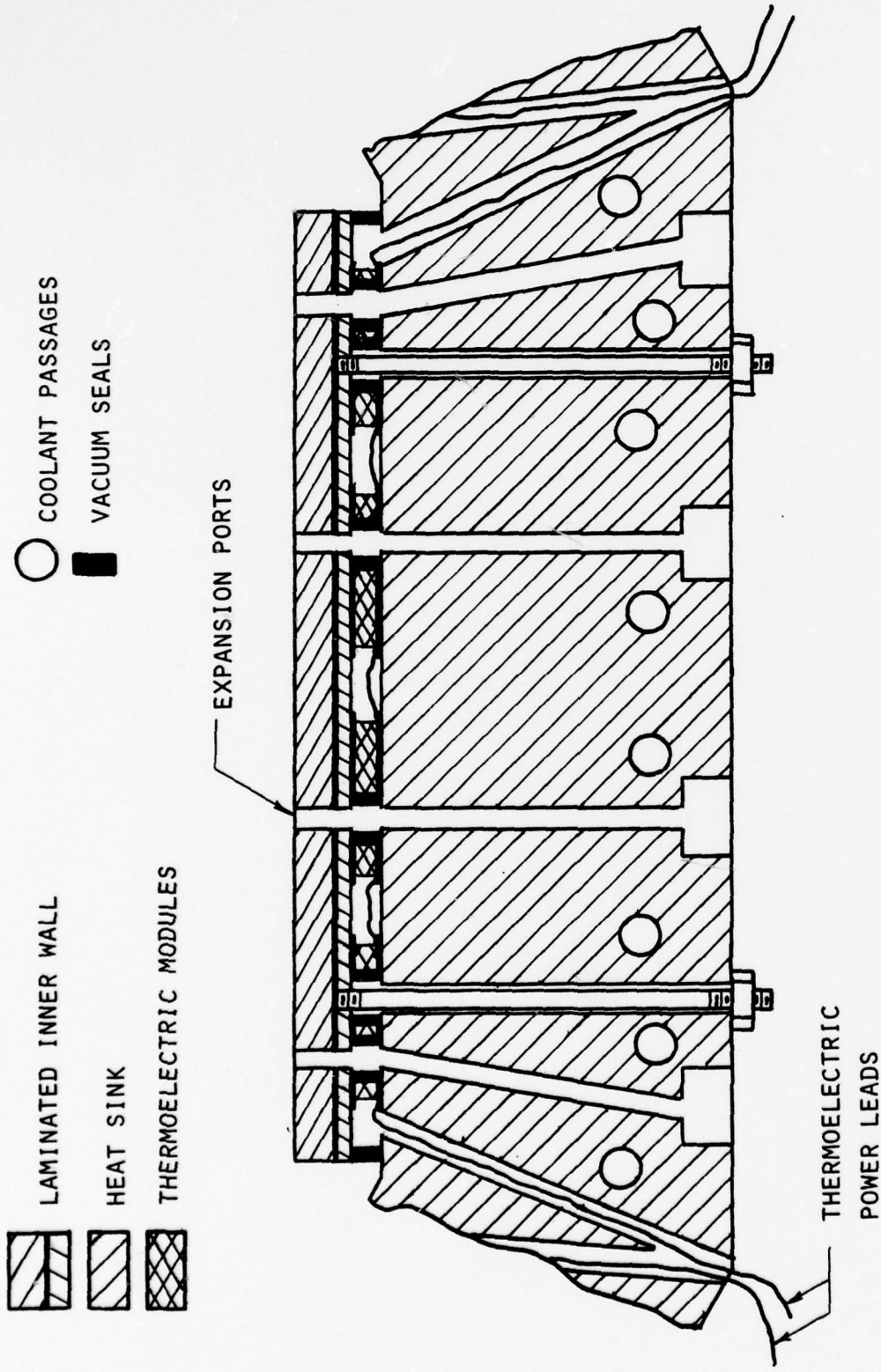
FIG 2. CROSS-SECTION OF CHAMBER WALL

○ COOLANT PASSAGES
■ VACUUM SEALS

EXPANSION PORTS

LAMINATED INNER WALL

HEAT SINK

THERMOELECTRIC MODULES

THERMOELECTRIC
POWER LEADS

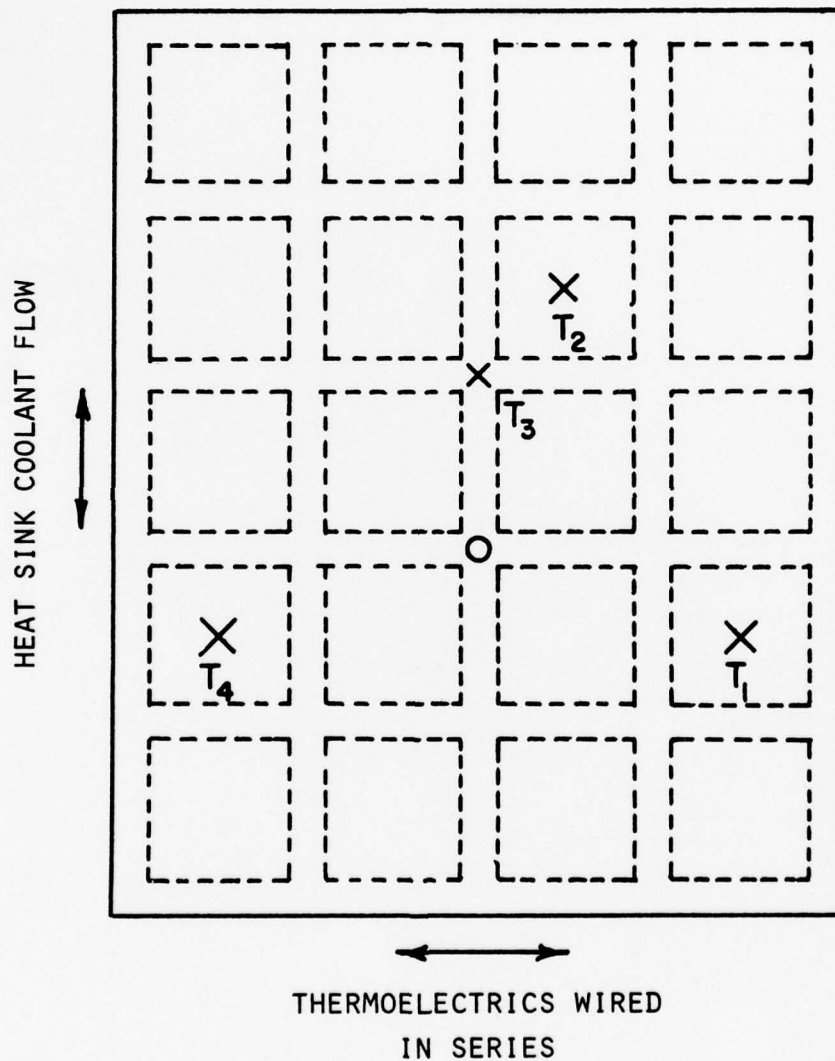✕ SURFACE THERMOCOUPLE

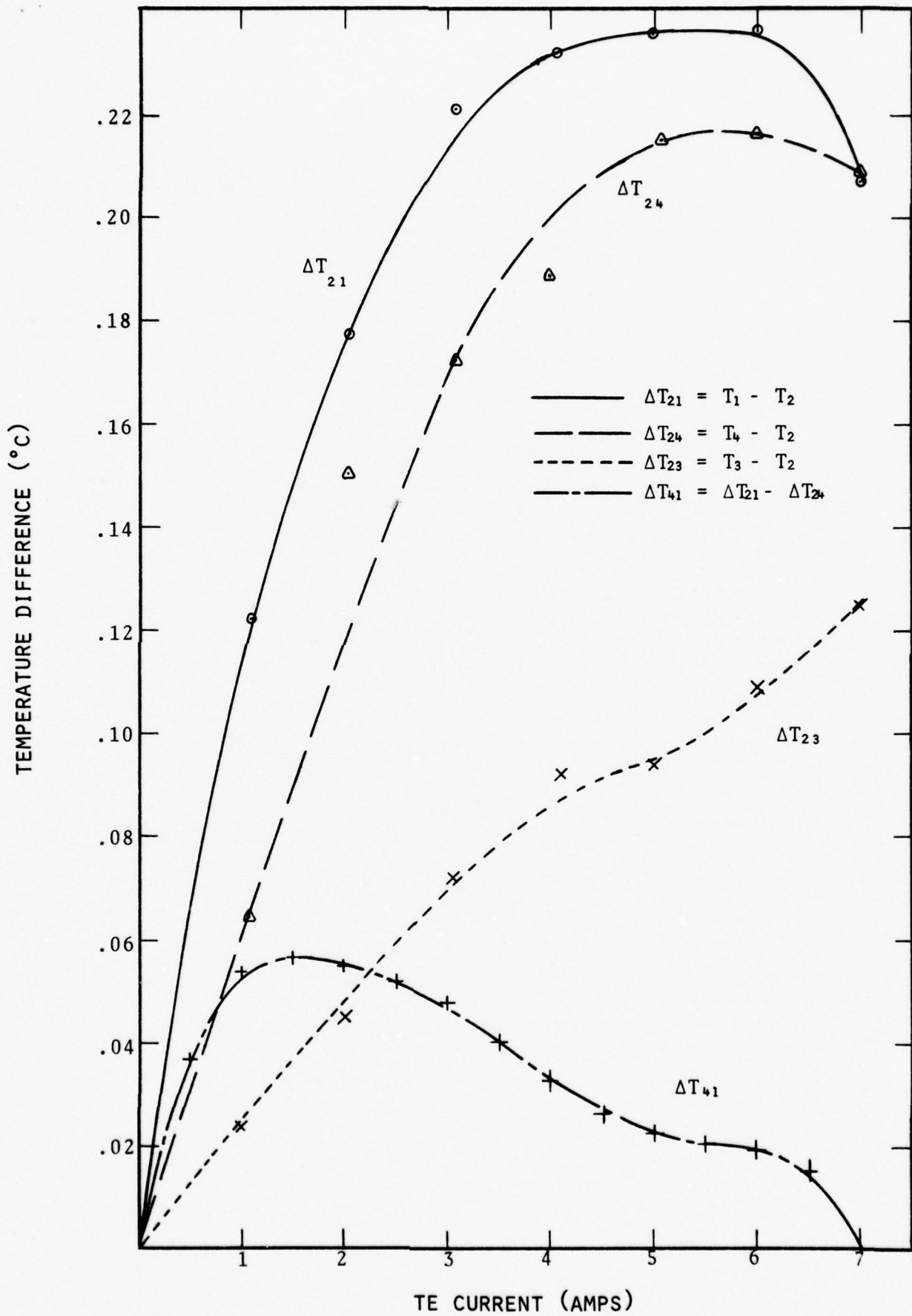⭕ TRANSISTOR THERMOMETER

FIG 3. LOCATION OF TEMPERATURE
SENSORS DURING THERMAL TESTS

FIG 4. INNER WALL SURFACE TEMPERATURE DIFFERENCES
VS THERMOELECTRIC CURRENT

NEW SIMULATION CHAMBER-ROMULUS ANALYSIS
OF EXPANSION MANIFOLD FLOW (1-8)

D. J. Schleuter - D. R. White

I.   Introduction

The purpose of this study is to adjust the design of the
expansion manifold to insure uniform volumetric flow from all in-
terior parts. Removal from the manifold system will be at four
equal spaced points around the chamber. Calculation will be based
on the flow requirements of a dry adiabatic expansion of 15°C/min
at room temperature and atmospheric pressure.

Interior expansion parts from a grid four parts wide and
nine parts high on each of the twelve side of the chamber side wall
section. Each minifold covers a grid four parts wide and three
high, so there are three manifolds required to cover each section.
The twelve manifolds surrounding the chamber at a given level are
all interconnected to increase pressure uniformity.

II. Calculations

A. Volumetric change per second associated with each mani-
fold.

Chamber volume per manifold is a triangular prism

$$V_o = 1/2 \ abh \qquad a=12in \ , \quad b=6.425in \ , \quad h=5.33in$$

$$V_o = 205.47in^3$$

$$V_2 = V_1 (T_1/T_2)^{\frac{1}{\gamma-1}}$$

$$V_2 - V_1 = V_1 [(T_1/T_2)^{\frac{1}{\gamma-1}} - 1]$$

$$T_1 = 20^{\circ}C = 293.16^{\circ}K \qquad T_2 = 19.75^{\circ}C = 292.91^{\circ}K$$

$$\gamma = 1.4 \qquad \text{adiabatic index for air}$$

$$V_1 = V_o = 205.47 \text{ in}^3$$

$$\Delta V_m = V_2 - V_1 = .439 \text{ in}^3/\text{sec per expansion manifold}$$

$$\Delta V_p = {}^{\Delta Vm}/12 = .036 \text{ in}^3/\text{sec per interior port}$$

B. Density of the air

$$\nu_1 = {}^{RT}1/P_1 \qquad R = 53.34 \frac{\text{ft-\#}}{\text{\# }^oR}$$

$$T_1 = 528 \ ^oR$$

$$P_1 = 14.0 \ \text{\#}/\text{in}^2$$

$$\nu_1 = 13.97 \ \text{ft}^3/\text{\#}$$

$$\nu_2 = \nu_1 (\frac{528}{527.55})^{2.5} = 14.00 \ \text{ft}^3/\text{\#}$$

$$\nu_{avg} = 1/2(\nu_2 + \nu_1) = 13.98 \ \text{ft}^3/\text{\#}$$

$$P = {}^{1}/\nu \ avg = .0715 \ \text{\#}/\text{ft}^3 = 4.138 \times 10^{-8} \text{\#}/\text{in}^3$$

C. Passages from interior surface to manifold entrance two
    passage configuartion shown in Fig. 1

Fig. la represents the
two center columns of
ports on a side while
Fig. lb represents the
two outside columns.
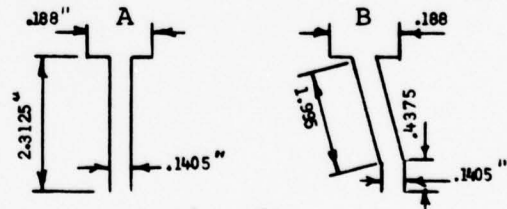
Fig 1

Kenematic viscosity of air $\nu = 1. \times 10^{-4} \ \text{ft}^2/\text{sec}$

air velocity in passage la

$$\nu_1 = \frac{\Delta V_p}{A} = \frac{.036}{\frac{\pi(.1405)^2}{4}} = 2.32 \ \text{in}/\text{sec}$$

$$Re = \nu_1 d/\nu = (2.32)(.1405)/(1.6 \times 10^{-4})(144) = 14.15$$

$$f = 64/Re = 4.52$$

passage length   L=2.3125 in

less factor (K)

entrance   K=.34

exit $K=(1-d_1^2/d_2^2)^2 = .20$

Total   K= .54

$$\Delta p = \frac{\rho f L v_1^2}{2dg} + \rho \frac{K v_1^2}{2g} \qquad g= 32.2 \text{ ft/sec}^2$$

$$= \frac{\rho v_1^2}{2g} [\frac{fL}{d} + K] = 2.16 \times 10^{-5} \#/\text{in}^2$$

The effective length of passage 16 is increased by 8 diameters
due to the bend

$$\Delta p = \frac{\rho v^2}{2g} [\frac{fL_e}{d} + K] = 2.16 \times 10^{-5} \#/\text{in}^2$$

$$p = 4.138 \#1/\text{in}^3$$

$$g = 32.2 \text{ ft/sec}^2$$

$$f = \frac{64}{Re} = \frac{64\nu}{\nu\alpha} =$$

$$\nu = 1.6 \times 10^{-4} \text{ft}^2/\text{sec}$$

$$v = \frac{4\Delta Vp}{\pi\alpha^2}$$

$$\Delta V_p = .036 \text{ in}^3/\text{sec}$$

$$L_e = 2.4325 + 8\alpha$$

$$K = .54$$

Substitute and solve forth order equation for d by iteration
d = .1579 in.

Therefore use #21 drill d = .159 in

D. Passages from entrance to manifold to horizontal collection
passage (Fig. 2)

Hole Diameters (Trial Sizes)

AG=BE=CF=DH=.188in

FD = .156in

GD = .222in

$$\Delta p(CF) = \Delta p(BE) = \Delta p(AG) = \frac{\rho f L v^2}{2gd}$$

Fig 2

$\rho = 4.138 \times 10^{-5} \#/in^3$ $\qquad$ $g = 386.4 \ in/sec^2$

$d = .188in$ $\qquad$ $L = .75 + 50d = 10.15$ $\qquad$ $v = 2.304 \times 10^{-2} in^2/sec$

$\Delta V_p = .036 in^3/sec$ $\qquad$ $v = \frac{4\Delta V_Q}{\pi \alpha^2} = 1.297 in/sec$

$$f = \frac{64}{R_e} = \frac{64v}{v\alpha} = 6.047$$

$\Delta p = 2.94 \times 10^{-5} \ \#/in^2$

$\Delta p(FD)$

d=.156in $\qquad$ L=.8+50d=B.6in

v=1.883in/sec $\qquad$ f=5.02

$\Delta p(FD) = 5.253 \times 10^{-5} \#/in^2$

$\Delta p(CD) = 8.2 \times 10^{-5} \#/in^2$

$$\Delta p(BE) = \Delta p(AE) = \frac{\rho f_{BE} L_{BE} v_{BE}^2}{2d_{BE}g} = \frac{\rho f_{AG} L_{AG} v_{AG}^2}{2d_{AG}g} + \frac{\rho f_{GE} L_{GE} v_{GE}^2}{2d_{GE}g}$$

$$f_{BE} = \frac{16v\pi d_{BE}}{Q_B} \qquad f_{AG} = \frac{16v\pi d_{AG}}{Q_A} \qquad f_{GE} = \frac{16v\pi d_{GE}}{Q_A}$$
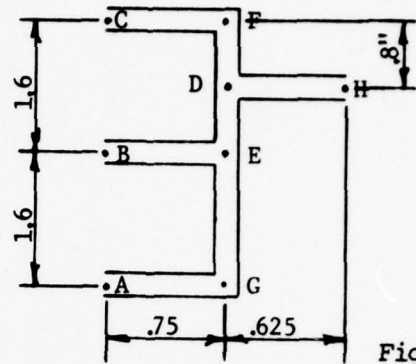
$$L_{BE} = (.75 + 50d_{BE}) \qquad L_{AG} = (.75 + 50d_{AG}) \qquad L_{GE} = (1.6 + 20d_{GE})$$

$$v_{BE} = \frac{4Q_B}{\pi d_{BE}^2} \qquad v_{AG} = \frac{4Q_A}{\pi d_{AG}^2} \qquad v_{GE} = \frac{4Q_A}{\pi d_{GE}^2}$$

Substituting $\quad \dfrac{L_{BE} \ Q_B}{d_{BE}^4} = \dfrac{L_{AG} Q_A}{d_{BE}^4} + \dfrac{L_{GE} Q_A}{d_{BE}^4}$

$$(.75 + 50d_{BE})d_{BE}^{-4}Q_B = \{(.75 + 50d_{AG})d_{AG}^{-4} + (1.6 + 20d_{GE}^{-4}\}Q_A$$

Requrie $\quad Q_A = Q_B \qquad d_{BE} = .188in \qquad d_{GE} = .222in$

then $d_{AG} = .212in \quad$ use #3 drill $d_{AG} = .213in$

$$\Delta p(BE) = \rho f_{BE} L_{BE} v_{BE}^2 / 2d_{BE}g$$

$$= 2.94 \times 10^5 \#/in^2$$

$$\Delta p(FD) = \Delta p(ED) = \frac{\rho f_{FD} L_{FD} v_{FD}^2}{2gd_{FD}} = \frac{\rho f_{ED} L_{ED} v_{ED}^2}{2gd_{ED}}$$

$$\frac{L_{FD}^- Q_C}{d_{FD}^4} = \frac{L_{ED}(Q_A + Q_B)}{d_{ED}^4}$$

$$L_{FD} = (.8 + 50d_{FD}) \qquad L_{ED} = (.8 + 50d_{ED})$$

$$2Q_C = Q_A + Q_B$$

$$(.8 + 50d_{FD})d_{FD}^{-4} = 2(.8 + 50d_{ED})d_{ED}^{-4}$$

$$d_{ED} = .222in$$

$d_{FD} = .177in \qquad$ #16 drill $\qquad \Delta p(FD) = 3.756 \times 10^{-5} \#/in^2$

E.   Horizontal collection passage (Fig. 3)

lengths AG,BH,CI,DJ,EK,FL=0.625in

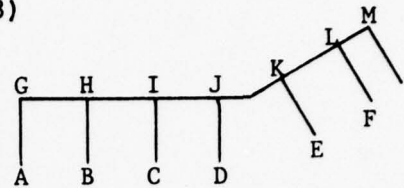GH = IJ = KL = 1.903 in; LM=.872 in

JK = 2.987 in; HI= 1.744 in

Fig 3

Assume diameters AG,BH,CI,DJ,EK & FL = 0.188 in

Assume diameter of horizontal collection passage = 1.250 in

Determine distribution of flow

$$\Delta P_{AG} = \frac{\rho f_{AG} L_{AG} v_{AG}^2}{2g d_{AG}} + \frac{\rho k v_{AG}^2}{2g} = 1.90 \times 10^{-6} \ \#/in^2$$

$Q = 3(.036) in^3/sec$

$L_{AG} = .625$ $K=1$ $d_{AG} = .188$ in

$\Delta P_G = [2.16 + 2.94 + 3.756 + .190] \times 10^{-5} = 9.046 \times 10^{-5} \ \#/in^2$

pressure drop from inside of chamber to horizontal

collection passage for $Q = .036 \ in^3/sec$

$$\Delta P_{GH} = \frac{\rho f_{GH} L_{GH} v_{GH}^2}{2g d_{GH}} = 8.463 \times 10^{-9} \#/in^2$$

$L_{GH} = 1.903$ in $d_{GH} = 1.250$ in $Q = 3(.036) in^3/sec$

$$\Delta P_{HI} = \frac{\rho f_{HI} L_{HI} v_{HI}^2}{2g d_{HI}} = 1.55 \times 10^{-8} \ \#/in^2$$

$L_{HI} = 1.744$ in $d_{\#J} = 1.250$ $Q = 6(.036) \ in^3/sec$

$\Delta P_I = 9.048 \times 10^{-5} \#/in^2$

$Q_{AG}/Q_{CI} = \Delta P_G/\Delta P_I = .9997$

$$\Delta P_{IJ} = \frac{\rho f_{Ij} L_{Ij} v_{Ij}^2}{2gd_{IJ}} = 2.538 \times 10^{-8} \text{ \#}/\text{in}^2$$

$$L_{IJ} = 1.903 \text{ in} \qquad d_{IJ} = 1.250 \qquad Q = 9(.036) \text{ in}^3/\text{sec}$$

$$\Delta P_J = 9.050 \times 10^{-5} \text{ \#}/\text{in}^2$$

$$Q_{AG}/Q_{DJ} = \Delta P_G/\Delta P_J = .9995$$

$$\Delta P_{jk} = \frac{\rho f_{jk} L_{jk} v_{jk}^2}{2gd_{jk}} = 2.310 \times 10^{-7} \text{ \#}/\text{in}^2$$

$$L_{JK} = 2.987 + 8(1.25) \qquad d_{jk} = 1.25 \qquad Q = 12(.036) \text{ in}^3/\text{sec}$$

$$= 12.987$$

$$\Delta P_K = 9.073 \times 10^{-5} \text{ \#}/\text{in}^2$$

$$Q_{AG}/Q_{EK} = \Delta P_G/\Delta P_K = .9970$$

$$\Delta P_{KL} = \frac{\rho f_{KL} L_{KL} v_{KL}^2}{2gd_{KL}} = 4.233 \times 10^{-8} \text{ \#}/\text{in}^2$$

$$L_{KL} = 1.903 \text{ in} \qquad d_{KL} = 1.250 \text{ in} \qquad Q = 15(.036) \text{ in}^3/\text{sec}$$

$$\Delta P_L = 9.077 \times 10^{-5} \text{ \#}/\text{in}^2$$

$$Q_{AG}/Q_{FL} = \Delta P_G/\Delta P_L = .9966$$

$$Q_{FL} = 1.003 \, Q_{AG}$$

which considering the accuracy of the calculatious is no significant change.

Remaining lines will be sized to keep differences insignificant

III Conclusions

The passage sizes calculated above should give an expansion which draws equal air volume through all internal parts with a variation of less than .3% between maximum and minimum single part flow rate.

AEROSOL LOSSES DURING PASSAGE THROUGH
THE CHAMBER INLET SYSTEM (1-8)

D. J. Schleuter - D. R. White

The purpose of this study is to determine the fraction of
aerosol particles lost during introduction of the sample into
the chamber sensitive volume. The inlet system consists of the
lowest expansion manifold with the top expansion manifold serv-
ing as the outlet. The flow is assumed to be laminar based on
the Reynolds number. Volumetric flows of 3 liter/sec and
10 liter/sec were studied as the two extremes. The expansion
manifold is broken up into four sections located symmetrically
around the chamber and each of these has symmetry about the cen-
tral inlet, therefore only one side of one section need be treated.

The flow velocity in each section of the manifold was first
determined based on one-eighth of the total flow entering and
being divided equally among the eighteen internal parts. The
flow velocity given by

$$v = Q/(\pi r^2)$$

where Q is the volumetric flow rate and r the tube diameter, was
used at each point to calculate the Reynolds number

$$Re = {}^{vd}/\nu$$

to verify the laminar flow assumption. d is the passage diameter
and ν is the kinematic viscosity.

Each individual section of passage within the manifold was
then considered individually and the constant μ, given by

$$\mu = {}^{Dx}/r^2 \bar{v}$$

where x is the passage length, r the radius, $\bar{v}$ is the mean fluid
or aerosol velocity and assumed to equal the flow velocity calcul-
ated above. The diffusion coefficient D was taken from Fuchs
(Mechanics of Aerosols, Pergamon Press, New York, 1964, p 184)
for particles with radii of 1.0, 0.1, 0.01 and 0.001 micron.

Using the appropriate value of μ the fraction of particles
of a given size passing through that section of manifold passage
was determined from the expression

$$\bar{n}/r_o = 1 - 2.56\mu^{2/3} + 1.2\mu + 0.177\mu^{4/3}$$

(Fuchs, p 205, Eq 39.3). The fractional concentrations of each section between the inlet and a particular interior port were then multiplied together to give a total effect. The results are listed in Tables 1 and 2.

Table 1 is for a total flow of 3 liter/sec while Table 2 is for 10 liters/sec. Each table is arranged in a 6 x 3 array of major divisions representing the eighteen interior ports. Column A is the ports closest to the inlet and column F those furthest from the inlet.
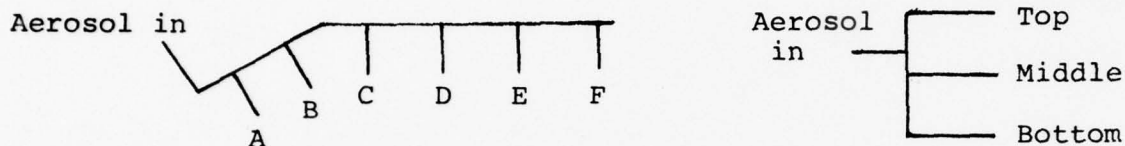
The three rows refer to the three levels of ports covered by one manifold. The results for each of the four particle sizes are given within each major division.

particle radius	A	B	C	D	E	F	
0	.4828	.4632	.4302	.4293	.4154	.3687	TOP
1	.9665	.9649	.9614	.9613	.9598	.9562	
01	.9977	.9976	.9974	.9973	.9972	.9970	
001	.9996	.9996	.9996	.9996	.9996	.9995	
0	.5429	.5210	.4837	.4828	.4671	.4333	MIDDLE
1	.9714	.9690	.9661	.9661	.9646	.9610	
01	.9980	.9979	.9977	.9976	.9975	.9973	
001	.9998	.9997	.9996	.9996	.9996	.9996	
0	.3538	.3394	.3151	.3146	.3044	.2823	BOTTOM
1	.9523	.9505	.9471	.9470	.9455	.9420	
01	.9966	.9966	.9964	.9962	.9962	.9960	
001	.9996	.9995	.9994	.9995	.9995	.9994	

TABLE 1

Fractional concentration of aerosol entering chamber

Flow rate 3 liters/sec

TABLE 2

Fractional concentration of aerosol entering chamber

Flow rate 10 liters/sec

Particle radius	A	B	C	D	E	F	
0	.72812	.71475	.69118	.69044	.68020	.65750	TOP
1	.98483	.98395	.98236	.98232	.98160	.98001	
01	.99893	.99892	.99881	.99880	.99876	.99865	
001	.99985	.99984	.99982	.99982	.99981	.99979	
0	.76339	.74938	.72466	.72389	.71316	.68936	MIDDLE
1	.98704	.98615	.98455	.98450	.98379	.98219	
01	.99913	.99637	.99626	.99895	.99891	.99610	
001	.99987	.99986	.99984	.99984	.99983	.99981	
.0	.63361	.62198	.60149	.60083	.59191	.57216	BOTTOM
.1	.97819	.97732	.97573	.97569	.97497	.97339	
.01	.99852	.99846	.99835	.99834	.99830	.99819	
.001	.99978	.99977	.99975	.99975	.99974	.99972	

APPENDIX D

"A DIGITAL CONTROL PROGRAM FOR AN EXPANSION CLOUD CHAMBER"

K. Menke and D. E. Hagen

The following is the outline of a paper presented at
the meeting of the Missouri Academy of Science describing
the computer program developed to control the optical
systems used to sense the cloud formation and development
within the chamber. The program has been tested using an
attenuation system operating in the visible red $(.63\mu)$
which permits the use of the attenuation system while the
Mie scattering of blue green light $(.488\mu)$ and flash
photographs of the cloud are also being acquired. The
program can also take the data required to obtain at drop
size spectrum of the cloud based on the Doppler frequency
shift of scattered laser light.

This program or a modification will be required to
control data acquisition during IR measurements in the
large simulation chamber.

A Digital Control Program for an Expansion Cloud Chamber

Kevin Menke and Donald Hagen

The Missouri Academy of Science Meeting, St. Louis, April, 1977

The purpose of this paper is to describe the methods used in a real time control and data acquisition program for a Cloud Simulation Chamber experiment.

The outline of the paper on slide one shows that first the elementary operation of the chamber will be discussed. The purpose of the program is to test several optical observation systems. Secondly these systems will be discussed. The third part of the paper shows the techniques used in the program.

The cloud simulation chamber may be thought of as a sealed metal canister. The canister is first filled with moist aerosol laden air. The contents are expanded, condensing the moisture on the aerosol.

Slide two shows the simulation chamber controlled by the Nova 840 minicomputer. The acquisitioning and control are those which are used in the program.

Slide three is a photograph of the Nova 840 and its peripherals. For this experiment data acquisition was done through a High Level Analog to Digital convertor as well as a Wide Range Analog to Digital convertor. Control is achieved through digital output.

The purpose of the program is to test four optical systems. These systems are shown in slide 4. They are:
1.) Attenuation - The light source is a light emitting diode. The information obtained is the clouds drop density and size.
2.) Doppler Shift - The light source is an argon-ion laser. The method informs one of the cloud's drop size spectrum.
3.) Mie Scattering - The light is supplied by the argon-ion laser. The information obtained is the drop size. The cloud must be monodisperse.
4.) Photography - One is able to count the drop density of the cloud.

Slide five shows the main parts of the multi-task fortran program called OPTTST (Optical Test). The program begins with the pre-expansion phase. The expansion initiates the tasks CAMERA, UCLOSE and STTORLD and follows with the post-expansion chores.

The time line of OPTTST (slide six) shows that during pre-expansion, time intervals for the expansion are accepted. The calculation constants needed in calculations during the post-expansion are read in. An initial set of data is recorded.

With the opening of the valve, task UCLOSE is initiated. It waits until time T1 has elapsed and then closes the expansion valve. Task CAMERA is also initiated. It waits until time T3 and begins taking

photographs. At each photo time task CAMERA is given control and the task closes the photomultiplier tube so that no damage is done to the measurement equipment due to the flash. The P-M tube is then opened after the picture has been taken. The task is done after a given number of photos have been taken. During the suspension of these tasks the program control is given to a main DO loop which reads data into data vectors and also signals the light beam oscillograph that data has been taken. Task STTORLD is initiated on the first loop to store doppler laser data on a binary file for future use.

The data loop will finish after 21 iterations (a time of T2 has elapsed). The post-expansion phase of the program calculates the pressure ratios and attenuation ratios. The results are immediately displayed on the CRT. One may also obtain a printout of the results of the expansion.

Some conclusions are that OPTTST shows that real time experiment programming is greatly simplified when one uses multi-tasking as a programming tool. One might as well point out that digital controlled experiments have great versatility as compared to analog controlled experiments. A wide variety of different experiments may be run by simply writing new soft ware.

.PAPER OUTLINE

1. CLOUD SIMULATION CHAMBER

2. TEST OPTICAL OBERVATION SYSTEMS

3. COMPUTER PROGRAM

DIGITAL OUTPUT MONITOR
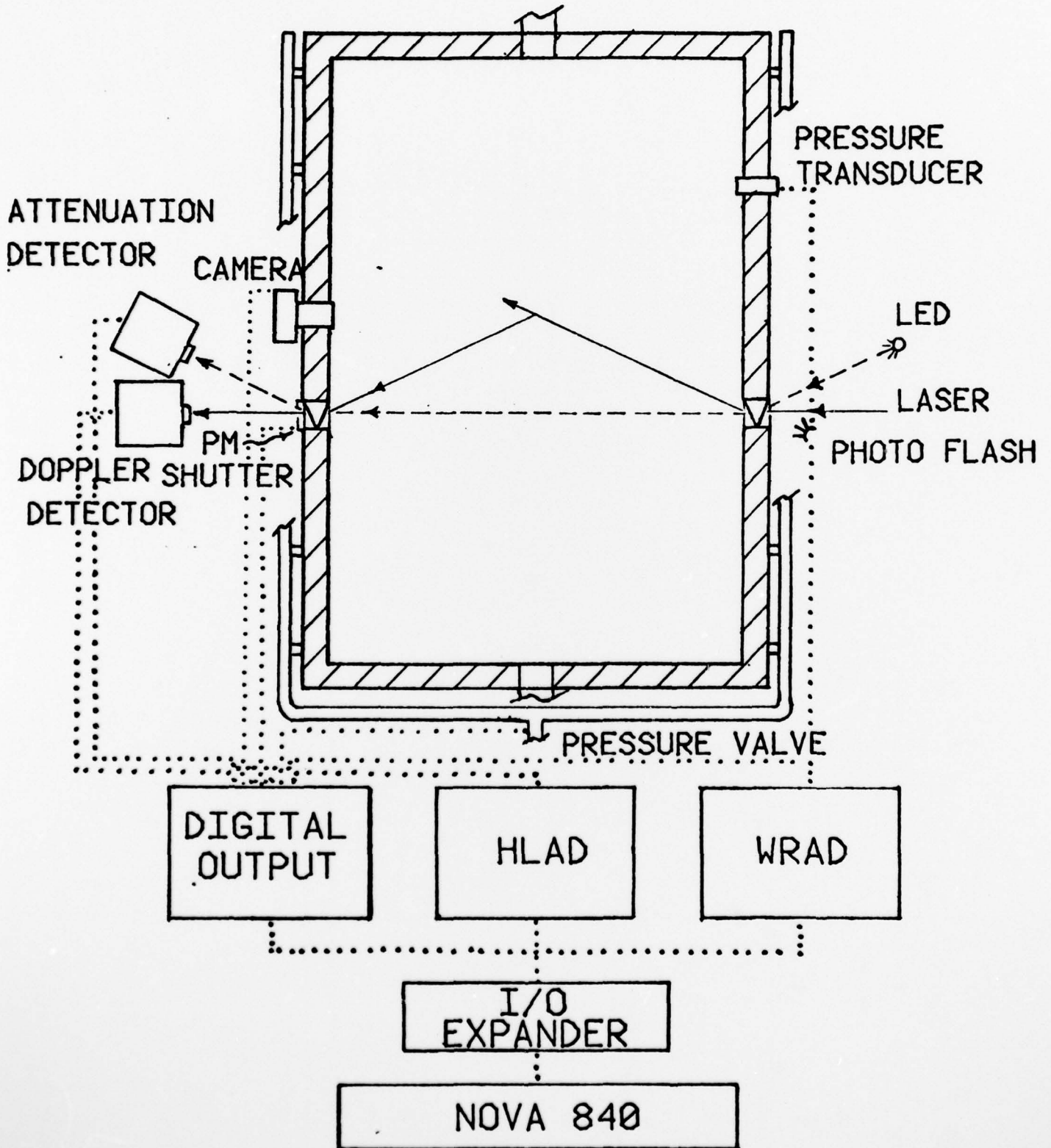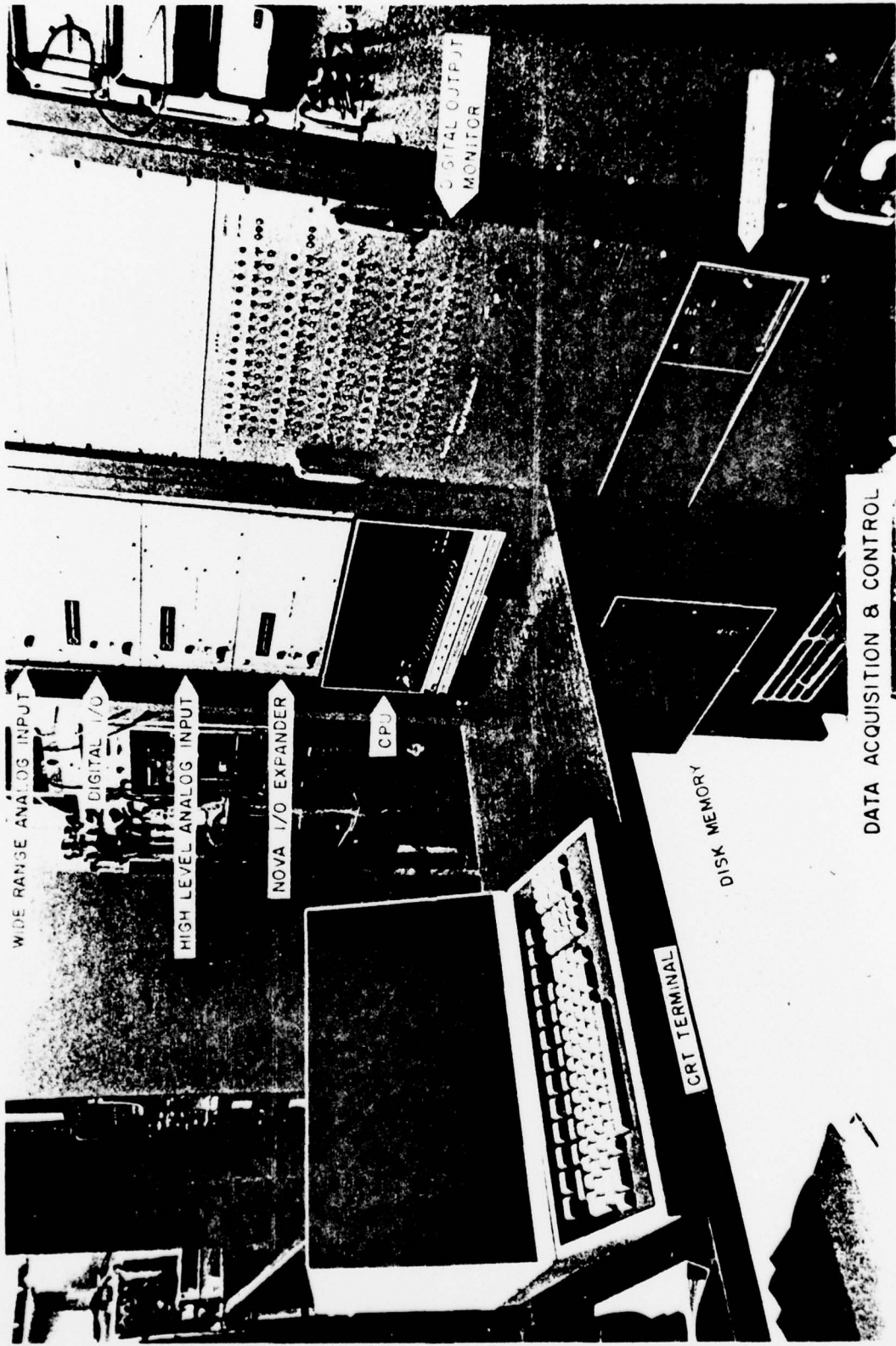
WIDE RANGE ANALOG INPUT

DIGITAL I/O

HIGH LEVEL ANALOG INPUT

NOVA I/O EXPANDER

CPU

CRT TERMINAL

DISK MEMORY

DATA ACQUISITION & CONTROL

AVAILABLE OPTICAL OBSERVATION METHODS

1. ATTENUATION

    A. LED

    B. DROP DENSITY / SIZE

2. DOPPLER SHIFT

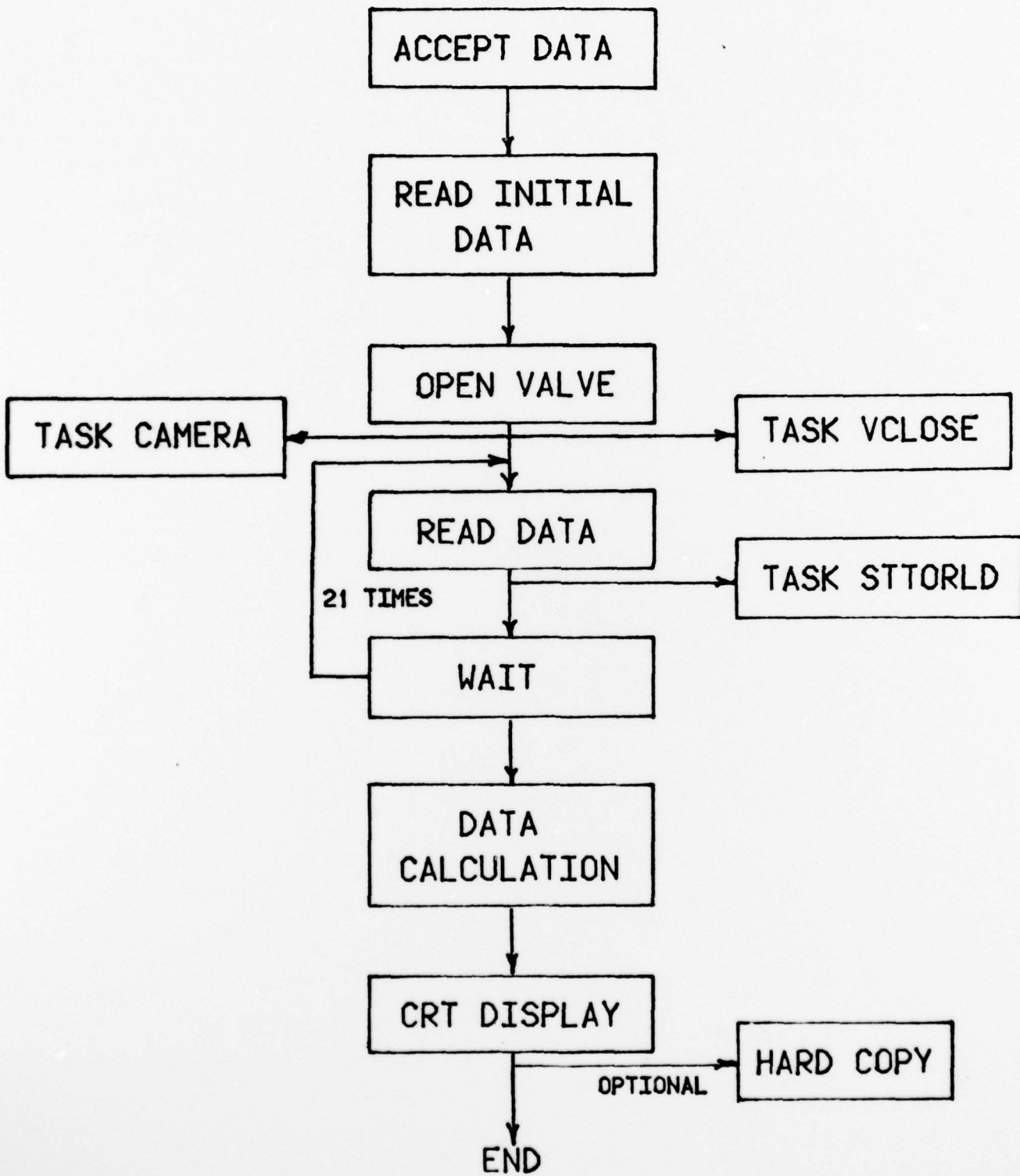   A. ARGON-ION LASER

    B. DROP SIZE SPECTRUM

3. MIE SCATTERING

    A. ARGON-ION LASER

    B. DROP SIZE - MONODISPERSE CLOUD

4. PHOTOGRAPHY

    A. FLASH LAMP

    B. DROP DENSITY

OPTTST FLOWCHART

OPTTST

SET DIGITAL DEVICES

ACCEPT TIME INTERVALS AND
                CALCULATION CONSTANTS

T0   INITIAL DATA – D0 –

OPEN VALVE – D1 –

– D2 –

READ DOPPLER DATA

T3   BEGIN TAKING PHOTOS

– DN –

PHOTO

– DN+1 –

STOP TAKING PHOTOS

– DN1 –

READ DOPPLER DATA

– DN1+1 –

– DN2 –

T1   **CLOSE VALVE**

– DN2+1 –

READ DOPPLER DATA

– DN3 –

– DN3+1 –

T2   STOP TAKING DATA

CALCULATE DATA AND DISPLAY
                ON CRT

PRINT OUT HARD COPY

.250 DRILL - .375 DP.
(2-REQ'D. @ 180°)
F.S. ONLY

2.250
2.255

#7(.2010) TAP DRILL - .500 DP.
1/4-20 TAP - .375 DP.
(12-REQ'D. EQ. SP.)
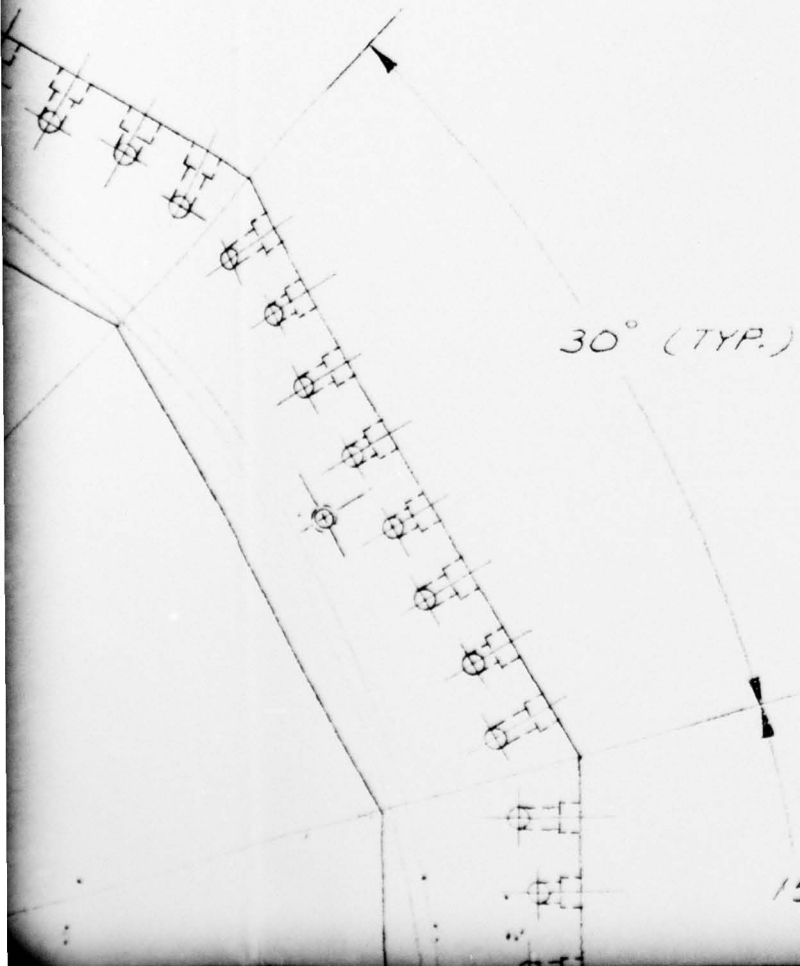(N.S. ONLY)

6.420
6.430

11.980
12.000

13.115 R.
13.125
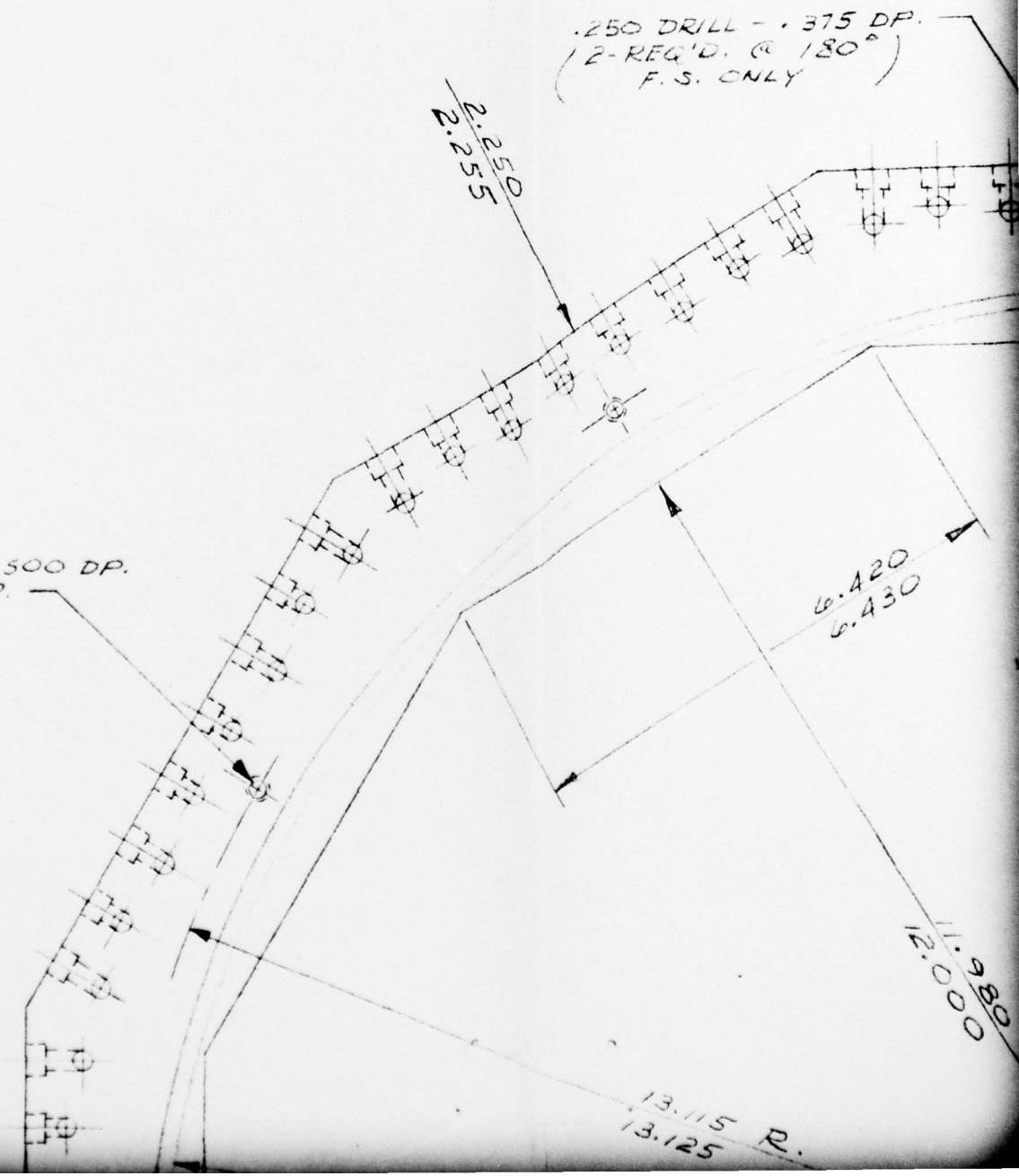
LL - .375 DP.
D. @ 180°
ONLY

€ COOLANT PASSAGE
(TYP.)

6.420
6.430

11.980
12.000 R

R.

2

PASSAGE

30° (TYP.)

15°

3

€ CHAMBER

12.550 R.
12.560

"A"

"A"

"O"- RING GROOVE
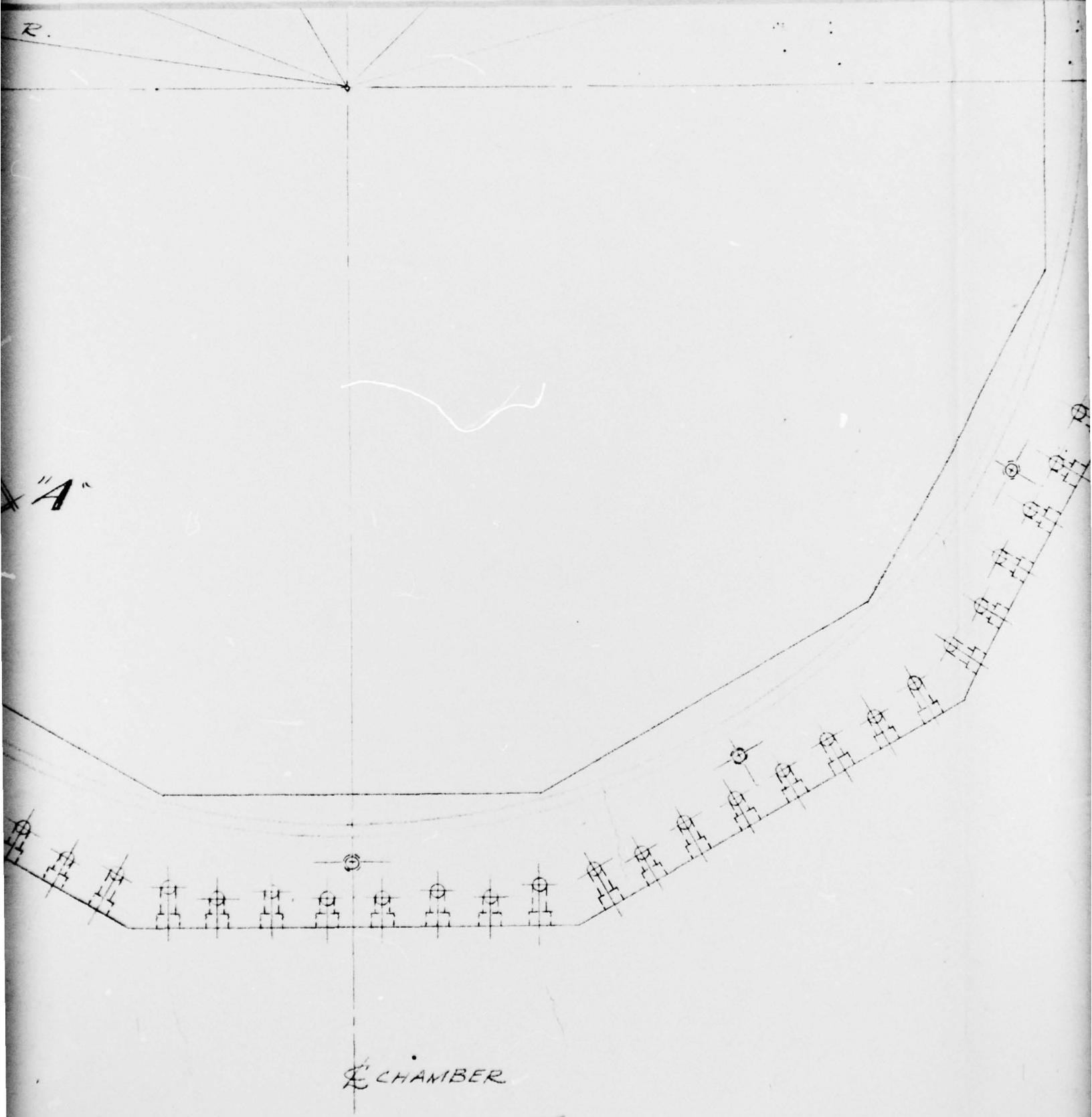(SEE SHEET 4 OF 4)
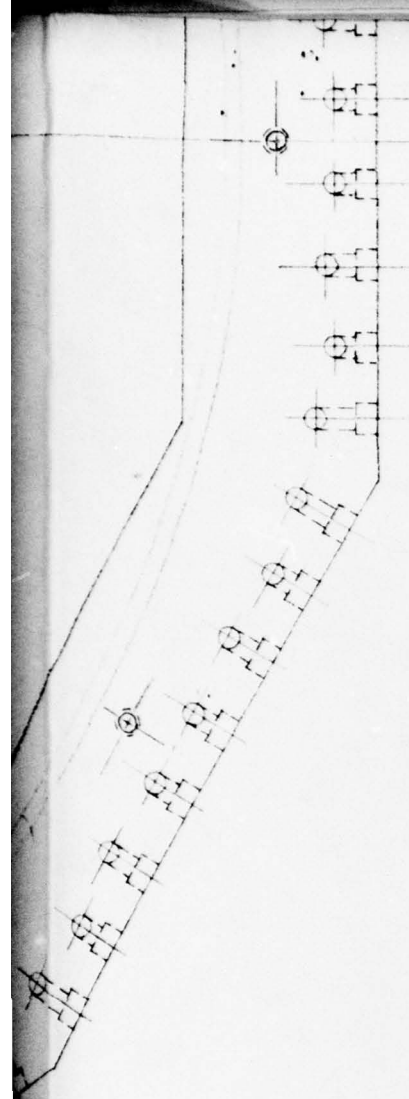
"F"

"F"

(SEE SHEET 4 OF 4)

4
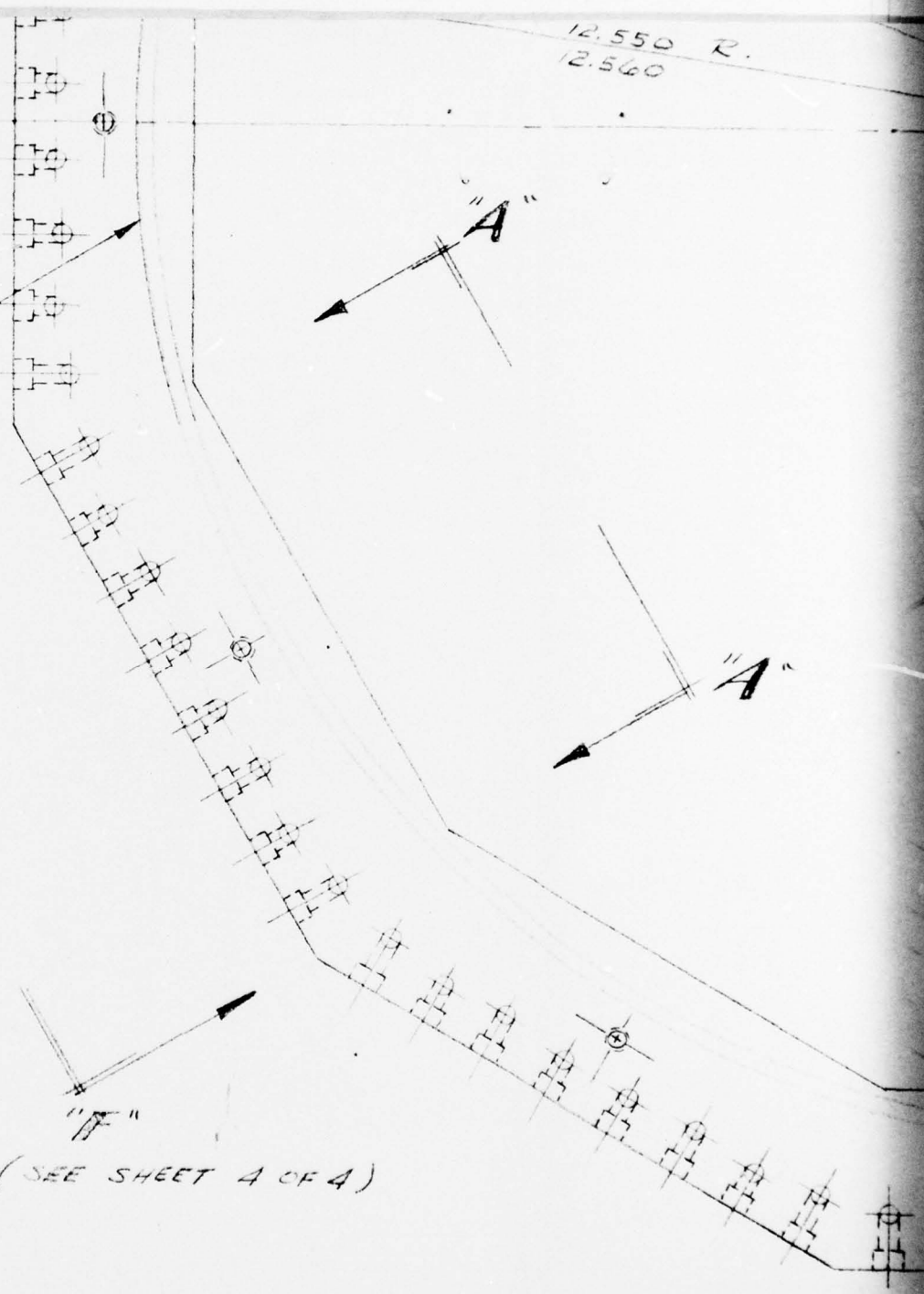
R.

"A"

℄ CHAMBER

5

PLAN VIEW

NOTE

1. COOLANT PASSAGES ARE
SHOWN ONLY FOR CLARITY.

UMR - GCCPR   SIMULATION PROJECT
CHAMBER SECTION (HEAT SINK)
ALUMINUM
SCALE : 1/2" = 1"
1/6/77
TOM SCHASTEEN, JR.

6